Journal of ELECTRONIC MATERIALS, Vol. 49, No. 4, 2020
https://doi.org/10.1007/s11664-019-07909-w

Evolution and Growth Mechanism of $Cu_2(In,Sn)$ Formed Between In-48Sn Solder and Polycrystalline Cu During Long-Time Liquid-State Aging

FEIFEI TIAN ,[1,2] XUEYONG PANG,[3] BO XU,[1] and ZHI-QUAN LIU[2,4,5,6]

1.—Nanjing Electronic Devices Institute, Nanjing 210016, China. 2.—Institute of Metal Research, Chinese Academy of Sciences, Shenyang 110016, China. 3.—School of Materials Science and Engineering, Northeastern University, Shenyang 110819, China. 4.—Shenzhen Institutes of Advanced Technology, Chinese Academy of Sciences, Shenzhen 518055, China. 5.—e-mail: zqliu@siat.ac.cn. 6.—e-mail: zhiquanliu@yahoo.com

Evolution of $Cu_2(In,Sn)$ formed between In-48Sn solder and polycrystalline Cu during long-time liquid-state aging was systematically investigated. During aging at 160°C up to 90 min, one IMC species, $Cu_2(In,Sn)$ was found, which showed two different morphologies, a coarse-grained $Cu_2(In,Sn)$ sublayer and a fine-grained Cu2(In,Sn) sublayer. The fine $Cu_2(In,Sn)$ grains had and always kept a granular morphology without any growth orientation. The morphology of coarse $Cu_2(In,Sn)$ grains evolved from poly-facet pyramidal-type without preferential orientation into hexagonal structure preferring only one elongated direction after aging up to 90 min. Electron beam backscattered diffraction revealed that coarse-grain $Cu_2(In,Sn)$ compound grew along [0001] axis and exposed {11-20} crystal planes. Growth mechanism of coarse $Cu_2(In,Sn)$ grains related closely to thermodynamic stability of hexagonal structure, which drove by reduction of surface energy from higher to lower, and first principles calculations verified that {11-20} crystal planes had the lowest surface energy. Fine $Cu_2(In,Sn)$ grains had a special growth mechanism at the root of coarse $Cu_2(In,Sn)$ grains compared to normal fine $Cu_2(In,Sn)$ grains underneath coarse $Cu_2(In,Sn)$ grains.

Key words: In-48Sn solder, polycrystalline Cu, $Cu_2(In,Sn)$, growth orientation

INTRODUCTION

It is an inevitable trend to use lead-free solder as a substitute for lead-containing solder in thevmicroelectronic field due to environmental and health problems. Amongst the Pb-free solder families, SnAgCu,[1–5] SnCu[6,7] and SnBi[8–10] solders were studied systematically and fully. Besides the above-mentioned Sn-based Pb-free solders, the binary eutectic In-48Sn solders exhibit a different character with the addition of In elemental species, such as lower melting temperature, better ductile properties and longer fatigue life.[11] According to our knowledge, Lin[12] and Chen[13] had studied the interfacial reactions between γ-$InSn_4$ solder and Cu substrate at 160°C for a long time, and far-reaching conclusions were drawn. However, different atomic percentage In-Sn solder systems and different characterizing methods were used, it was reasonable to obtain different conclusions. It is known that In element acting as a reacting species in a ternary Sn-In-Cu system makes the interfacial reaction between In-48Sn solder/Cu more complex, and meanwhile Cu-In based crystal structure intermetallic compounds (IMCs) would be possible to form.

It is known that an IMC layer acting as an important metallurgical bonding layer has obvious

(Received May 9, 2019; accepted December 17, 2019; published online January 2, 2020)

effects on the mechanical properties of solder joints and their serving reliability, especially textured IMC may have great influence on the electronic and mechanical properties of solder joints. Xian et al.[14] had studied bulk Sn-xCu alloys and in Sn-0.7 wt.%Cu/Cu solder joints under different cooling rates and Cu contents and elucidated the crystal growth mechanisms of primary Cu_6Sn_5 with preferred growth. Li et al.[15] studied the Sn3.5Ag/polycrystalline Cu interface during long-time liquid-state aging and revealed that Cu_6Sn_5 grains showed strong texture. However, according to our knowledge, no researcher has paid attention to the evolution and preferred growth of interfacial IMC during long-time liquid-state aging in the In-48Sn/polycrystalline Cu system. And our previous study mainly focused on short-time interfacial reaction and solid-state aging in the In-48Sn/Cu system,[16,17] and long-time liquid-state aging has never been reported. Therefore, a deep study on evolution and growth orientation of IMC at In-48Sn/polycrystalline Cu interface during long-time liquid-state aging is necessary.

In this study, a layer to layer top-view technique was used to reveal the evolution $Cu_2(In,Sn)$ IMC at an In-48Sn/polycrystalline Cu interface, EBSD was conducted to investigate preferential orientation of $Cu_2(In,Sn)$ after long-time liquid-state aging, surface energy calculations according to first-principles were conducted to verify the easily exposed crystal surface further, and for which the growth mechanism was analyzed in detail.

EXPERIMENTAL PROCEDURES

Aging Sample Preparation

Firstly, the oxygen-free, high purity polycrystalline copper plates (> 99.995%) were cut by an electro-discharging machine to a size of $4 \times 4 \times 4$ mm^3. The Cu surfaces were ground with grade SiC papers successively and polished carefully with 1 μm and 0.5 μm diamond paste and then rinsed in acetone, distilled water, and dried. Secondly, the solder used in this study was In-48Sn alloy, which was prepared by high purity In and Sn elements (> 99.99%) with multi-melting in a vacuum melting oven. In-48Sn solder foils were rolled into a thickness of about 200 μm by a manual rolling mill, and whose length and width were in accordance with Cu substrate. Wetting samples were prepared by putting the In-48Sn thin foil dipping tacflux012 (purchased from Indium corporation) on its surface on polished Cu substrates and soldered at 160°C ranging from 5 min to 90 min on a heat table, and then the formed solder joint was cooled in air up to ambient temperature. Afterwards, the samples were cleaned ultrasonically in acetone for 5 min to dissolve the remaining flux on the sample surfaces, and the sample is shown in Fig. 1.

IMC Morphology Observation

The soldered samples were ground with grade SiC papers successively and carefully polished by BUEHLER polishing suspension with 0.05 μm Al_2O_3 powder to prepare cross-sectional scanning electron microscopy (SEM) samples. And a layer to layer etched technique was used to clearly reveal the top-view morphologies of IMCs with 20% H_2O_2 + 80% CH_3COOH (vol.%) etchant solution, which has the advantage of low etching rate and less effect on the Cu substrate. The solidified In-48Sn solder after aging was mechanically ground away to about 50 μm, and then the solder joints was etched layer to layer. The cross-sectional and top-view SEM samples were rinsed with distilled water in an ultrasonic bath for 10 min to clear away Al_2O_3 powder suspension and residual etchant solution, and then dried in air. All clean samples were observed with LEO super35 and Quanta 600 SEMs with energy-dispersive x-ray spectroscopy (EDS) system for compositional analyses. And the thickness of IMC layers was measured using image analyses software as described earlier.[18]

EBSD Analysis on Crystallographic Orientation

As the preferential growth of coarse-grain $Cu_2(In,Sn)$ IMC was observed on polycrystalline Cu substrate during long-time liquid-state aging, EBSD was performed to study the crystallographic orientation using a LEO super35 SEM. Since each elongated IMC grain is a single crystal, the Kikuchi patterns coming from selected spots of elongated grains are feasible to determine the crystallographic orientation. Owing to the EBSD method is very sensitive to the roughness degree of the sample surface, thus, after SEM observations the samples were properly ion-milled again by LEICA EM RES101 to get a smooth surface for EBSD experiments, the ion milling voltage was 1.2 keV and milling time was 3 min.

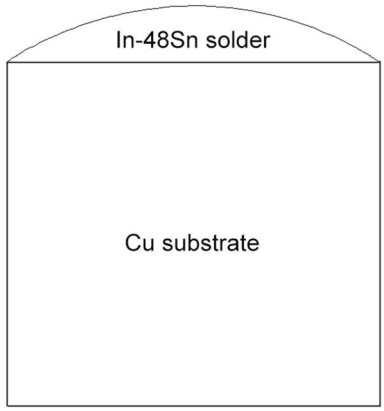

Fig. 1. A schematic diagram of cross-sectional image of the sample

First-Principles Calculations on Surface Energy

First-principles calculations were conducted using VASP[19] with PAW[20,21] pseudo potentials. The exchange–correlation potential was described by the generalized gradient approximation functional of PBE.[22] The plane wave cut-off energy was set at 500 eV. The k-point sampling based gamma-centered Monkhorst–Pack scheme[23] was used for the structural relaxations and the geometry optimization process was performed using a conjugate-gradient algorithm until the final force on each atom was less than 0.01 eV/Å.

RESULTS

Cross-Sectional Morphology Evolution of IMC

Cross-sectional SEM images of the In-48Sn/Cu interface reveals the evolution of interfacial IMC, it can be clearly seen that one kind of IMC layer with a uniform phase contrast was formed after liquid-state aging at 160°C for a different time, as shown in Fig. 2. Moreover, it can be obviously seen that the thickness and grain size of IMC at the solder side increase with the increment of liquid-state aging time, and the thickness of interfacial IMC layers measured using image analyses software was 2.38 μm, 6.04 μm and 9.87 μm, respectively, in Fig. 2. However, at the solder/IMC interface, more and more coarsening IMC grains spall from the IMC layer into In-48Sn solder after long-time liquid-state aging, as shown in Fig. 2c. According to our previous study[16] on spalling mechanism of interfacial IMCs at the In-48Sn solder and single-crystalline Cu interface, it is known that two kinds of continuous IMC layers: $Cu(In,Sn)_2$ and $Cu_2(In,Sn)$ were formed after reflowing at 160°C for 5 s, then after reflowing at 160°C for 60 s, most of $Cu(In,Sn)_2$ grains had spalled into the solder and less of them could be observed at the interface area, $Cu_2(In,Sn)$ phase was the dominated IMC at the interface. In this paper, liquid-state aging at 160°C for longer time more than 5 min, $Cu_2(In,Sn)$ could be the dominated IMC at the interface in an In-48Sn/Cu system, and composition analyses were further carried out using EDS in the following section.

EDS Analysis of Interfacial IMCs

A layer to layer top-view etched technique was used to reveal IMC morphologies at the interface of In-48Sn solder and polycrystalline Cu clearly, afterwards corresponding elemental EDS analysis was carried out to verify the IMCs formed after long-time liquid-state aging, as shown in Fig. 3. One kind of IMC layer with a uniform phase contrast revealed in Fig. 2 shows two different morphologies, a coarse-grained sublayer and a fine-grained sublayer. And the corresponding EDS analysis shows the coarse-grained IMC sublayer consists of 64.52%Cu, 14.74%In, and 20.73%Sn, which corresponds to 65Cu-15In-20Sn (at.%), and the fine-grained IMC sublayer consists of 70.99%Cu,11.00%In, and 18.01%Sn, which corresponds to 71Cu-11In-18Sn (at.%), as shown in Fig. 3c and d respectively. Based on previous study[16,24] on phase identification and morphology characterization of interfacial IMCs formed in an In-48Sn solder/single-crystalline and polycrystalline Cu system aging at 160°C for 5 s-60 s, it is known that the coarse-grained IMC sublayer and the fine-grained IMC sublayer have the same Cu_2In hexagonal crystal structure with similar elemental compositions during long-time liquid-state aging at 160°C on polycrystalline Cu substrate in this paper. Therefore, it can be concluded that one IMC species, $Cu_2(In,Sn)$ was found, which shows two different morphologies, a coarse-grained sublayer and a fine-grained sublayer.

Morphology Evolution of Fine-Grain $Cu_2(In,Sn)$

Figure 4 top-view SEM images show morphology evolution of fine $Cu_2(In,Sn)$ grains on

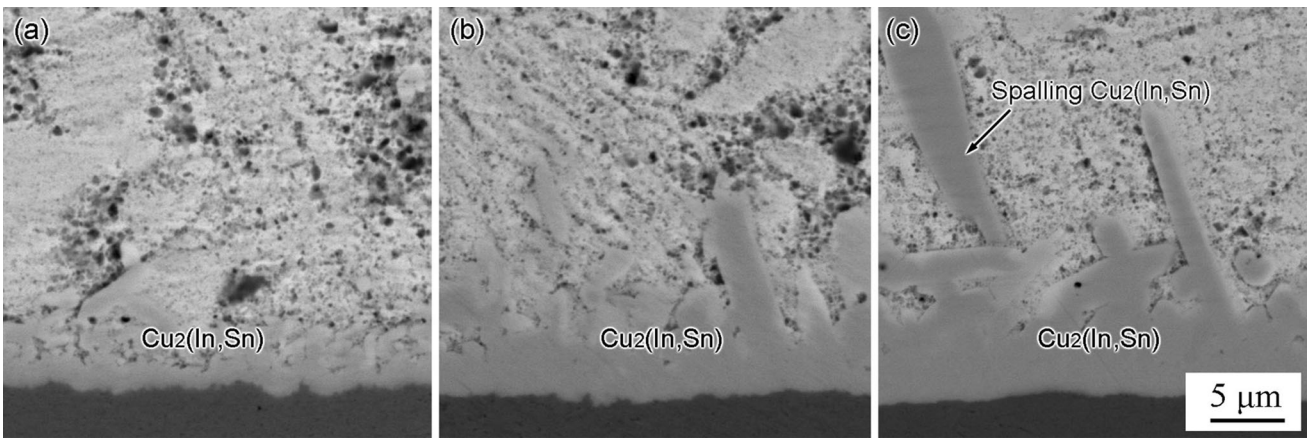

Fig. 2. Cross-sectional SEM images showing morphology evolution of duplex structure $Cu_2(In,Sn)$ after liquid-state aging for different times at 160°C: (a) 5 min; (b) 30 min; (c) 90 min

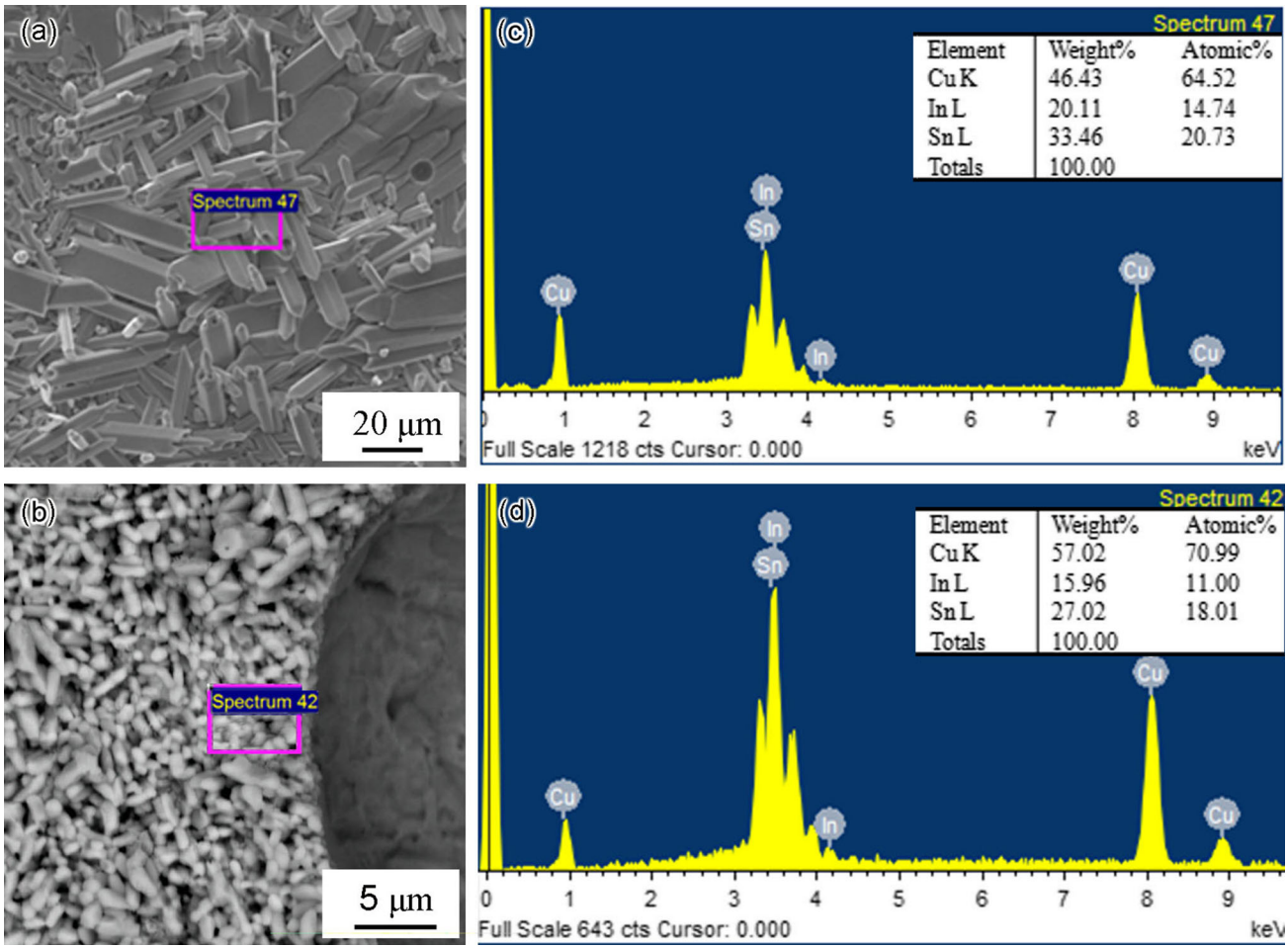

Fig. 3. EDS analysis of interfacial IMCs between In-48Sn solder and polycrystalline Cu after liquid-state aging at 160°C for 90 min: (a) coarse-grain $Cu_2(In,Sn)$; (b) fine-grain $Cu_2(In,Sn)$; (c) EDS analysis of coarse-grained IMC sublayer from Fig. 3(a); (d) EDS analysis of fine-grained IMC sublayer from Fig. 3(b)

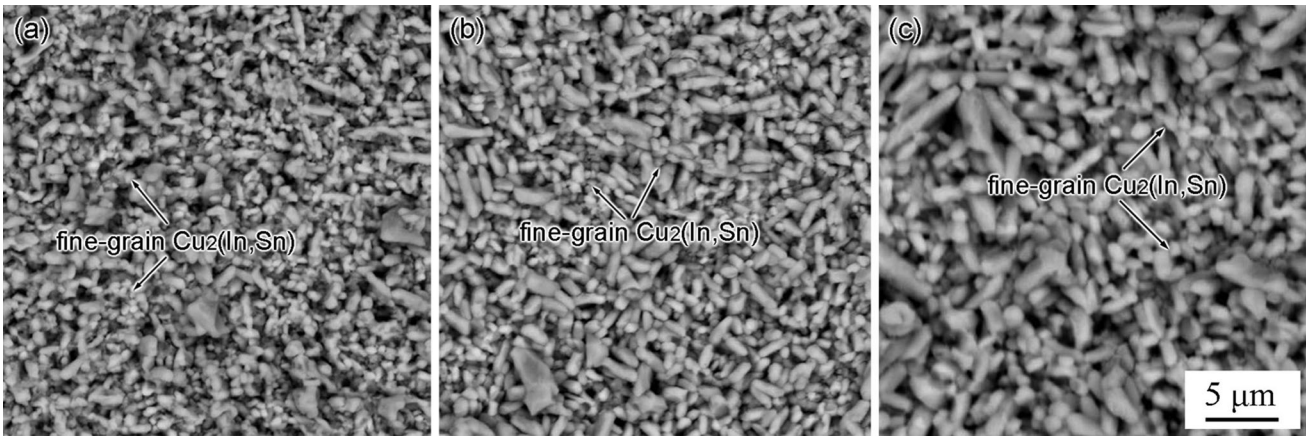

Fig. 4. Top-view SEM images showing morphology evolution of fine-grain $Cu_2(In,Sn)$ after liquid-state aging for different times at 160°C: (a) 5 min; (b) 30 min; (c) 90 min

polycrystalline Cu substrates after liquid-state aging at 160°C for different times. From Fig. 4, it can be clearly seen that the fine $Cu_2(In,Sn)$ grains have granule-type morphology with smaller grain size, and distributes homogeneously on the entire polycrystalline Cu substrates. Figure 4a and b reveal the morphology evolution of fine-grain $Cu_2(In,Sn)$ during liquid-state aging at 160°C for 5 and 30 min, respectively. It can be seen that fine-grain $Cu_2(In,Sn)$ grains increased slightly with the

same granular morphology. Further increase of liquid aging time up to 90 min results in bigger grain size of the fine $Cu_2(In,Sn)$ grains as shown in Fig. 4c. It is known that the fine $Cu_2(In,Sn)$ grains have and always keep a granular morphology, for which the grain size increases from sub-micrometer to micrometer during long-time liquid-state aging.

Morphology Evolution of Coarse-Grain $Cu_2(In,Sn)$

Figure 5 top-view SEM images show morphology evolution of coarse $Cu_2(In,Sn)$ grains on polycrystalline Cu substrates after liquid-state aging at 160°C for different times. Coarse $Cu_2(In,Sn)$ grains show poly-facet pyramidal-type structure with sharp edges in initial 5 min liquid-state aging, and each coarse grain has no obvious preferential growth, as shown in Fig. 5a. And then after liquid-state aging to 30 min, part of poly-facet pyramidal-type coarse $Cu_2(In,Sn)$ grains evolve into hexagonal grains, which prefer only one elongated direction with rod-type core at the tip of coarse $Cu_2(In,Sn)$ grains, as shown in Fig. 5b. Besides that, the remaining coarse $Cu_2(In,Sn)$ grains still keep poly-facet pyramidal-type structure with increasing grain size. For further liquid-state aging up to 90 min, all coarse $Cu_2(In,Sn)$ grains evolve into hexagonal crystal structure with hexagonal pyramidal-type core at the tip of coarse $Cu_2(In,Sn)$ grains, which prefer only one elongated direction, as shown in Fig. 5c. Another interesting phenomenon that should be paid attention to is that many poly-facet and hexagonal coarse $Cu_2(In,Sn)$ grains have a hollow core at the tip when liquid-state aging up to 30 min and 90 min, which will be discussed later.

EBSD Conduction on Coarse-Grain $Cu_2(In,Sn)$

Top-view SEM images show that coarse $Cu_2(In,Sn)$ grains evolve into hexagonal crystal structures, and for which growth prefers only one elongated direction after liquid-state aging at 160°C up to 90 min, which implies that there exist a special growth orientation of coarse $Cu_2(In,Sn)$ grains on polycrystalline Cu substrates. To verify this, EBSD experiments were performed on coarse $Cu_2(In,Sn)$ grains, as shown in Fig. 6. Since each preferential orientation, elongated coarse $Cu_2(In,Sn)$ grain is a single crystal, Kikuchi patterns from selected spots of coarse-grain $Cu_2(In,Sn)$ compound are enough to determine crystallographic orientation. Kikuchi pattern from elongated coarse $Cu_2(In,Sn)$ grains and a live description of 3D orientation illustration of coarse $Cu_2(In,Sn)$ crystal on polycrystalline Cu are displayed in Fig. 6a. It was found that the preferential growth of coarse-grain $Cu_2(In,Sn)$ compound grew along the [0001] direction and exposed the {11-20} crystal planes. Moreover, magnified top-view SEM images clearly reveal that coarse $Cu_2(In,Sn)$ grains evolve into hexagonal crystal structure with hexagonal pyramidal-type core at the tip of coarse $Cu_2(In,Sn)$ grains, and which prefer only one elongated direction aligning along the [0001] direction, as shown in Fig. 6b and c. Moreover, the hollow core at the tip of coarse $Cu_2(In,Sn)$ grains is also observed, and the melting direction is opposite to the [0001] crystal growth direction. According to Xian's[14] study on hexagonal Cu_6Sn_5 crystal growth mechanism during solidification and Frank's[25] study on capillary equilibria of dislocated crystals, they linked the formation of hollow-core rod-like crystals to an axial screw dislocation where the core remelted when the strain energy of the dislocation core exceeded the new surface energy required to create a hollow, the above hollow formation mechanism also applied to this situation, and further study will go on but not elucidate more in this study.

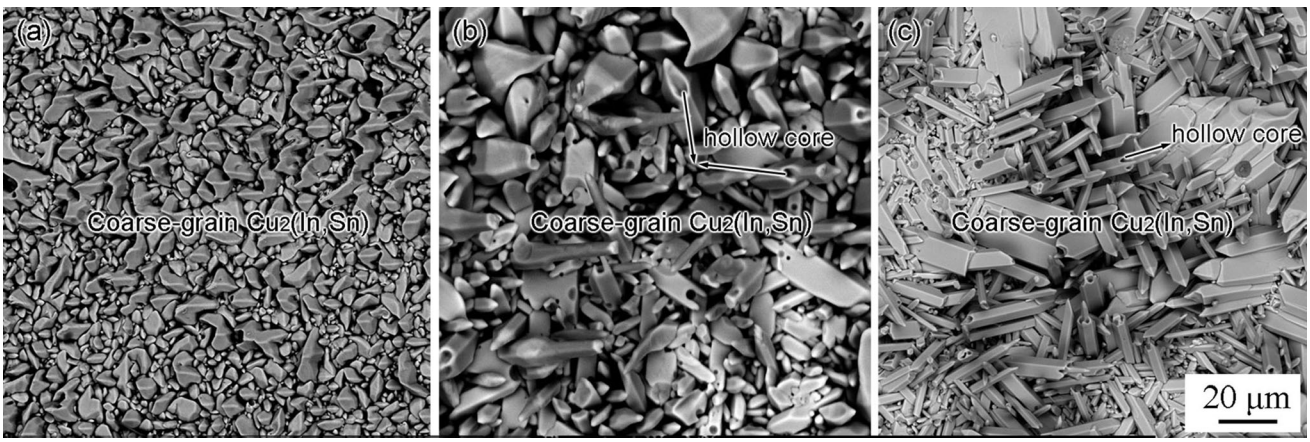

Fig. 5. Top-view SEM images showing morphology evolution of coarse-grain $Cu_2(In,Sn)$ after liquid-state aging for different times at 160°C: (a) 5 min; (b) 30 min; (c) 90 min

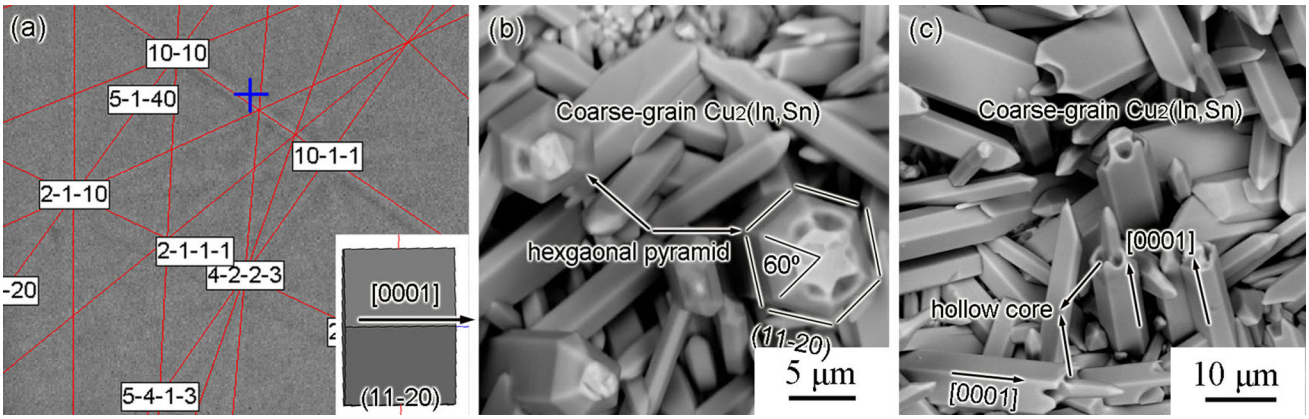

Fig. 6. (a) Kikuchi pattern of coarse Cu_2(In,Sn) grains on polycrystalline Cu substrate with 3D orientation illustration; (b) and (c) Top-view SEM images of coarse Cu_2(In,Sn) grains after liquid-state aging at 160°C for 90 min

DISCUSSION

Growth Mechanism of Coarse-Grain Cu_2(In,Sn)

In this paper, although fine-grain Cu_2(In,Sn) compound was formed on polycrystalline Cu substrate directly, interestingly it is the coarse-grain Cu_2(In,Sn) but not fine-grain Cu_2(In,Sn) that show certain regularity and preferential growth on polycrystalline Cu substrate during long-time liquid-state aging, which has never been reported by other researchers. It is known that the occurrence and sequence of IMC formation are determined by the highest driving force and the minimum Gibbs energy naturally. Lee et al.[26] successfully predicted the first formation of IMC at the interfaces between Cu substrate and Sn-Pb, Sn-Bi and Sn-Zn binary eutectic solders. However, due to the lack of related thermodynamic data of IMC in In-48Sn/Cu system, it was difficult to prove the formation sequence of IMC in In-48Sn/Cu system, especially Cu_2(In,Sn) has coarse- and fine-grain duplex structural sublayers. Their studies only concluded that Cu_6Sn_5 IMC could not form first at an In-48Sn/Cu interface. Therefore, it could be deduced that the coarse-grain Cu_2(In,Sn) compound nucleated first with relatively regular poly-facet morphologies during wetting reaction between In-48Sn solder and polycrystalline Cu substrate. According to Che et al.'s study,[27] it is known that Cu_2In has a hexagonal structure with lattice constants of $a = b$=0.4292 nm, c = 0.5232 nm, $\alpha = \beta$=90°, and γ = 120°. According to the rule of thermodynamics, the change of surface energy of coarse Cu_2(In,Sn) grains from higher surface energy with poly-facet pyramidal-type morphology to lower surface energy with hexagonal structure growing is an inevitable trend after long-time liquid-state aging. Due to thermodynamic stability of hexagonal crystal structure, coarse Cu_2(In,Sn) grains will keep hexagonal structure and grow aligning along the [0001] direction after long-time liquid-state aging.

To verify the above viewpoint further, first-principles calculations on (0001), (10-10) and (11-20) crystal surface structures of Cu_2In unit cell were conducted using VASP[19] with PAW[20,21] pseudo potentials, and the methodology of first-principles calculations was described in detail earlier. The surface energy in present calculations, $E_{surf(hkl)}$, was calculated from following equation:

$$E_{(\mathrm{hkil})\mathrm{surf}} = \frac{E_{(\mathrm{hkil})\mathrm{tot}} - n * E_{\mathrm{unit}}}{2A}. \quad (1)$$

Here, A is the unit area of surface structure, $E_{(\mathrm{hkil})\mathrm{tot}}$ and E_{unit} represent the total energy of the surface structure with Miller index (hkil) and the energy of Cu_2In unit cell, respectively. Moreover, atomic model of Cu_2In unit cell and schematic illustrations of the (0001), (10-10) and (11-20) surface structures are shown in Fig. 7.

According to Eq. 1, the surface energies of (0001), (10-10) and (11-20) planes were calculated as shown in Table I.

In Table I, (10-10) surface structure with different exposing atoms has two calculating results designating as $(10\text{-}10)_I$ and $(10\text{-}10)_{II}$ respectively, and the average value is 0.85 J/m^2. Therefore, the (11-20) plane has the lowest surface energy, and intersecting angle between two adjacent (11-20) planes of {11-20} family of crystal planes is 60° or 120°. Moreover, [0001] direction is normal to the (11-20) plane. {10-10} crystal planes may also be likely to grow stably after long-time liquid-state aging, but do not occur in this study. From the above experimental results and calculating analysis, it can be safely concluded that coarse Cu_2(In,Sn) grains prefer to growing along [0001] direction and exposing {11-20} crystal planes, which keep hexagonal structure after liquid-state aging at 160°C up to 90 min or longer.

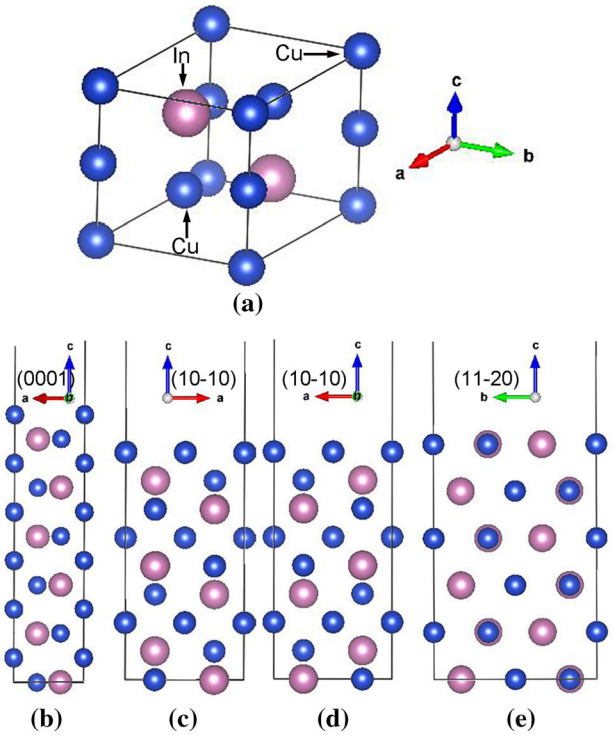

Fig. 7. (a) Atomic model of Cu_2In unit cell (the blue and pink spheres are Cu and In atoms as indicated by arrows, respectively), (b) schematic illustration of the (0001) surface structure, (c) and (d) schematic illustration of the (10-10) surface structure with different exposing atoms respectively, (e) schematic illustration of the (11-20) surface structure.

Table I. Surface energy of (0001), (10-10) and (11-20) planes

Plane	Energy (eV)	Area (Å^2)	Surface energy (J/m^2)
(0001)	− 57.03	4.47 × 3.87	1.56
$(10\text{-}10)_I$	− 56.16	5.38 × 4.47	0.72
$(10\text{-}10)_{II}$	− 75.355	5.38 × 4.47	0.98
(11-20)	− 113.68	5.38 × 7.75	0.72

Growth Mechanism of Fine-Grain $Cu_2(In,Sn)$

Besides fine $Cu_2(In,Sn)$ grains distributed on the entire polycrystalline Cu substrate as revealed in Fig. 4, one interesting phenomenon should be paid attention to that some fine $Cu_2(In,Sn)$ grains were formed in-between roots of coarse $Cu_2(In,Sn)$ grains in initial 5 min liquid-state aging as displayed in the circles of Fig. 8a. Further liquid-state aging at 160°C up to 30 min, the same growth phenomenon of fine $Cu_2(In,Sn)$ grains was also observed. Fine $Cu_2(In,Sn)$ grains were formed in-between roots of coarse $Cu_2(In,Sn)$ grains, as shown in circles of Fig. 8b, meanwhile, the normal fine $Cu_2(In,Sn)$ grains underneath coarse $Cu_2(In,Sn)$ grains were also observed as shown at the upper-right corner of Fig. 8b, whose growth mechanism was discussed in detail according to our previous Cr-marker experiment[28] that fine-grain $Cu_2(In,Sn)$ underneath coarse-grain $Cu_2(In,Sn)$ was generated from the later solid interfacial reaction between coarse-grain $Cu_2(In,Sn)$ and Cu substrate and here we did not elucidate further. The above phenomenon implies that the fine $Cu_2(In,Sn)$ grains have a special growth mechanism at the root of coarse $Cu_2(In,Sn)$ grains compared to the normal fine $Cu_2(In,Sn)$ grains underneath coarse $Cu_2(In,Sn)$ grains.

Cross-sectional SEM images could elucidate the growth mechanism of fine-grain $Cu_2(In,Sn)$ grains at the root of coarse $Cu_2(In,Sn)$ grains clearly, as shown in Fig. 9. It should be of attention that there exists In-48Sn solder in the interfacial IMC layer, as indicated by arrows in Fig. 9. According to the indication of arrows in the magnified inset at the upper-right corner, the diffusing direction of In-48Sn solder could be clearly seen. Due to existing grain boundary groves and continuous dissolution of Cu into liquid In-48Sn solder as well as the lift force of liquid solder, coarse $Cu_2(In,Sn)$ grains could spall into the solder. Thus the coarse $Cu_2(In,Sn)$ grains would be not compact and there exists a grain gap not a grain boundary between two adjacent coarse $Cu_2(In,Sn)$ grains, which can be proved by the enveloped In-48Sn solder in Fig. 9. At aging temperature, liquid In-48Sn solder at the interface between In-48Sn solder and interfacial IMC could still provide In and Sn for reaction, and the grain gaps between coarse $Cu_2(In,Sn)$ grains indicated by two blank ellipses in the inset would act as a quick transport channel for elemental diffusion.

Thus, a reasonable assumption for the growth mechanism of fine $Cu_2(In,Sn)$ grains at the root of coarse $Cu_2(In,Sn)$ grains could be made that the grain gaps in-between coarse $Cu_2(In,Sn)$ grains acting as a quick transport channel for liquid In-48Sn solder, which accumulate at the interphase boundary of coarse-grain $Cu_2(In,Sn)$ sublayer and Cu substrate, then In and Sn atoms react with Cu atoms to form a fine-grain $Cu_2(In,Sn)$ sublayer. Partial chemical reaction (2) takes place at the grain boundaries in-between roots of coarse $Cu_2(In,Sn)$ grains. Therefore, fine $Cu_2(In,Sn)$ grains have and always keep a granular morphology, and for which grain size is much smaller than that of coarse $Cu_2(In,Sn)$ grains.

$$In_{diffuse} + 2Cu_{surface} = Cu_2In_{fine} \quad (2)$$

CONCLUSIONS

In summary, evolution of $Cu_2(In,Sn)$ IMC formed between In-48Sn solder and polycrystalline Cu during liquid-state aging at 160°C up to 90 min was systematically investigated using a layer to layer top-view technique in this paper. The following conclusions were drawn, focusing on the morphology evolution of $Cu_2(In,Sn)$ IMC after long-time

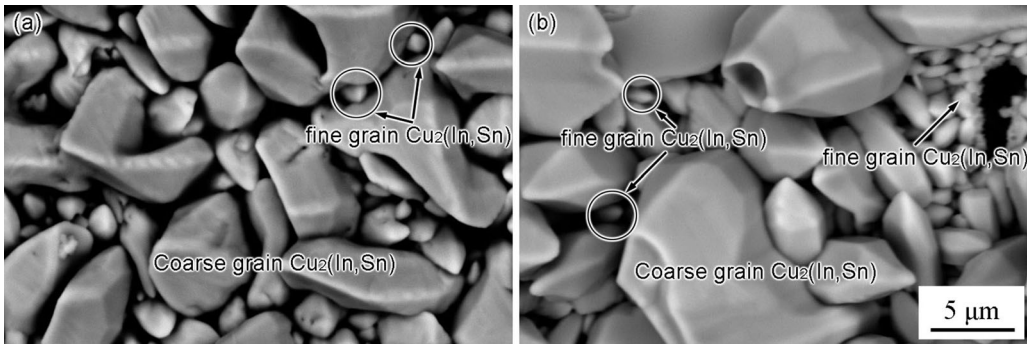

Fig. 8. Top-view SEM images showing morphology evolution of coarse-grain $Cu_2(In,Sn)$ and fine-grain $Cu_2(In,Sn)$after liquid-state aging for different times at 160°C: (a) 5 min; (b) 30 min

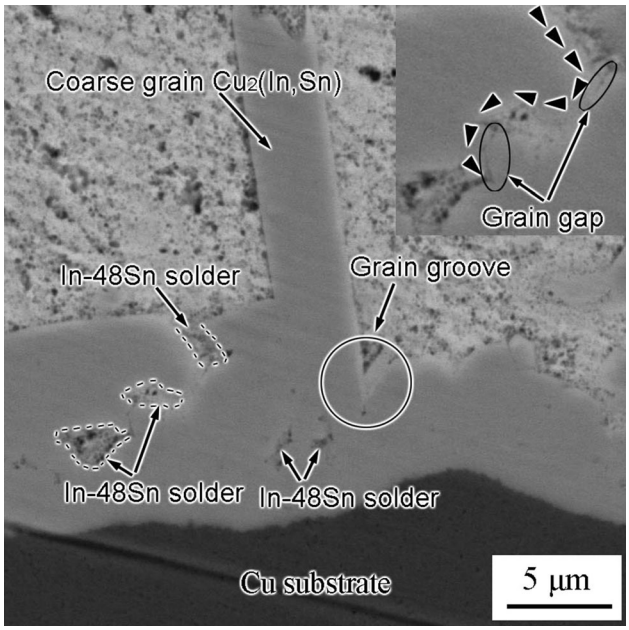

Fig. 9. Cross-sectional SEM images showing morphology evolution of coarse-grain $Cu_2(In,Sn)$ and fine-grain $Cu_2(In,Sn)$ after liquid-state aging at 160°C for 90 min

liquid-state aging, the preferential orientation of coarse $Cu_2(In,Sn)$ grains, surface energy of easily exposing crystal planes based on first-principles calculations, as well as the growth mechanism of coarse-grain and fine-grain $Cu_2(In,Sn)$ sublayers:

1. One dominated IMC species, $Cu_2(In,Sn)$ with two different morphologies, a coarse-grained sublayer and a fine-grained sublayer, was observed accompanying by spalling of coarse $Cu_2(In,Sn)$ grains at In-48Sn/polycrystalline Cu interface during liquid-state aging at 160°C up to 90 min.
2. Morphology evolution showed that fine $Cu_2(In,Sn)$ grains had and always kept a granular morphology without any growth orientation, which distributed homogeneously with slightly increasing grain size changing from sub-micrometer to micrometer during long-time liquid-state aging.
3. Morphology evolution showed that poly-facet pyramidal-type coarse $Cu_2(In,Sn)$ grains without preferential growth were revealed in initial 5 min liquid-state aging, then part of poly-facet pyramidal-type grains evolved into hexagonal, elongated grains with preferential growth after aging to 30 min and the remaining grains' morphology unchanged, then finally all coarse $Cu_2(In,Sn)$ grains evolved into hexagonal structural after aging up to 90 min.
4. EBSD revealed that the elongated coarse $Cu_2(In,Sn)$ grains grew along the [0001] axis and exposed {11-20} crystal planes.
5. Coarse-grain and fine-grain $Cu_2(In,Sn)$ sublayers have different growth mechanisms, respectively. Growth mechanism of coarse $Cu_2(In,Sn)$ grains related closely to thermodynamic stability of hexagonal structure, which was driven by reduction of surface energy from higher to lower, and first-principles calculations verified that {11-20} planes had the lowest surface energy of about 0.72 J/m^2.
6. Grain gap in-between coarse $Cu_2(In,Sn)$ grains acting as a quick transport channel dominated over the growth mechanism of fine $Cu_2(In,Sn)$ grains at the root of coarse $Cu_2(In,Sn)$ grains, and fine-grain $Cu_2(In,Sn)$ underneath coarse-grain $Cu_2(In,Sn)$ was generated from the later solid interfacial reaction between coarse-grain $Cu_2(In,Sn)$ and Cu substrate.

ACKNOWLEDGMENTS

This work was financially supported by the National Key R&D Program of China (Grant No. 2017YFB0305700) and the fundamental research funds for the Central Universities (Grant No. N160208001).

REFERENCES

1. M.Y. Xiong and L. Zhang, *J. Mater. Sci.* 54, 1741 (2019).
2. Satyanarayan and K.N. Prabhu, *Mater. Sci. Technol.* 29, 1430 (2013).
3. D. Tian and T. Kutilainen, *J. Electron. Mater.* 32, 152 (2003).

4. Y. Tian, Y. Wang, F. Guo, L.M. Ma, and J. Han, *J. Electron. Mater.* 48, 2770 (2019).
5. S. Narayan and K.N. Prabhu, *Mater. Sci. Technol.* 29, 464 (2013).
6. M. Hasnine and M.J. Bozackg, *J. Electron. Mater.* 48, 3970 (2019).
7. G.Y. Liu, S.X. Jin, and L.K. Grechcini, *Mater. Sci. Technol.* 33, 1907 (2017).
8. H.W. Miao, J.G. Duh, and B.S. Chiou, *J. Mater. Sci. Mater. Electron.* 11, 609 (2000).
9. L. Yang, L. Zhu, Y. Zhang, P. Liu, N. Zhang, S. Zhou, and L. Jiang, *Mater. Sci. Technol.* 34, 992 (2018).
10. Q. Hongbo, L. Xinghe, and Y. Wu, *J. Electron. Mater.* 48, 3410 (2019).
11. V.G. Shepelevich, O.V. Gusakova, E.L. Koukharenko, and S.V. Husakova, *J. Mater. Sci.* 54, 2577 (2019).
12. S.K. Lin and S.W. Chen, *J. Mater. Res.* 21, 1712 (2006).
13. S.W. Chen and S.K. Lin, *J. Mater. Res.* 21, 3065 (2006).
14. J.W. Xian, S.A. Belyakov, M. Ollivier, K. Nogita, H. Yasuda, and C.M. Gourlay, *Acta Mater.* 126, 540 (2017).
15. M.Y. Li, M. Yang, and J.Y. Kim, *Mater. Lett.* 66, 135 (2012).
16. F.F. Tian, Z.Q. Liu, P.J. Shang, and J. Guo, *J Alloys Compd.* 591, 351 (2014).
17. F.F. Tian, C.F. Li, M. Zhou, and Z.Q. Liu, *J. Alloys Compd.* 740, 500 (2018).
18. P.J. Shang, Z.Q. Liu, and D.X. Li, *Acta Mater.* 57, 4697 (2009).
19. G. Kresse and J. Furthmüller, *Phys. Rev. B* 54, 11169 (1996).
20. P.E. Blöchl, O. Jepsen, and O.K. Andersen, *Phys. Rev. B* 49, 16223 (1994).
21. G. Kresse and D. Joubert, *Phys. Rev. B* 59, 1758 (1999).
22. J.P. Perdew, K. Burke, and M. Ernzerhof, *Phys. Rev. Lett.* 77, 3865 (1996).
23. H.J. Monkhorst and J.D. Pack, *Phys. Rev. B* 13, 5188 (1976).
24. F.F. Tian and Z.Q. Liu, *J. Alloys. Compd.* 588, 662 (2014).
25. F.C. Frank, *Acta Cryst.* 4, 497 (1951).
26. B.J. Lee, N.M. Hwang, and H.M. Lee, *Acta Mater.* 45, 1867 (1997).
27. G.C. Che and M. Ellner, *Powder Diffr.* 7, 107 (1992).
28. F.F. Tian, P.J. Shang, and Z.Q. Liu, *Mater. Lett.* 121, 185 (2014).